

Article

# Removal of Tramp Elements within 7075 Alloy by Super-Gravity Aided Rheorefining Method

Lei Guo, Xiaochun Wen, Qipeng Bao and Zhancheng Guo \*

State Key Laboratory of Advanced Metallurgy, University of Science and Technology Beijing, Xueyuan Road No. 30, Haidian District, Beijing 100083, China; leiguo@ustb.edu.cn (L.G.); james365183262@163.com (X.W.); baoqipeng123@163.com (Q.B.)

\* Correspondence: zcguo@ustb.edu.cn; Tel.: +86-135-2244-2020

Received: 15 July 2018; Accepted: 3 September 2018; Published: 6 September 2018



**Abstract:** An investigation was made on the super-gravity aided rheorefining process of recycled 7075 aluminum alloy in order to remove tramp elements. The separation temperatures in this study were selected as 609 °C, 617 °C and 625 °C. And the gravity coefficients were set as 400 G, 700 G, 1000 G. The finely distributed impurity inclusions will aggregate to the grain boundaries of Al-enriched phase during heat treatment. In the field of super-gravity, the liquid phase composed of tramp elements Zn, Cu, Mg et al. will flow through the gaps between solid Al-enriched grains and form into filtrate. Both the weight of filtrate and removal ratio of tramp element improved with the increase of gravity coefficient. The total removal ratio of tramp element decreased with the fall of temperature due to the flowability deterioration of liquid phase. The time for effective separation of liquid/solid phases with super-gravity can be restricted within 1 min.

**Keywords:** super-gravity; rheorefining; aluminum alloy; tramp element; separation

## 1. Introduction

Aluminum and its alloys are important metallic materials in modern industry due to their high specific strength, corrosion resistance and good formability. And they can be considered as sustainable materials due to the little loss of quality when being recycled. The energy consumption of recycling aluminum scrap is only about 5% of that producing primary aluminum from bauxite using molten salt electrolysis method [1]. The production of primary aluminum is energy intensive and causing heavy emission of CO<sub>2</sub>. Thus, the production of secondary aluminum from recycled aluminum scrap has both economic and environmental benefits. However, those tramp elements (Fe, Si, Mg, Zn, Cu, Mn, Cr, etc.) exist in the recycled aluminum alloy scraps have to be eliminated or reduced before producing secondary aluminum alloys. The development of sorting technology in solid state can help to adjust the content of aluminum alloy scraps nowadays. Still, the accumulation of trace elements especially as Fe, Mn and Cr after repetitive reuse is the main problem. The removing effect of Fe, Mn, Cr elements was qualitatively proved in this study, and the detailed migration behavior of those three kinds of element will be further investigated in our later works.

The molten metal refining processes can be mainly classified into four types: (1) electrochemical refining (electrolytic refining), (2) physical refining (vacuum refining), (3) chemical refining (refining with fluxes [2,3]), (4) metallurgical refining (refining based on phase diagrams). However, only the metallurgical refining process features high efficient and large quantity. Based on the classification of the metallurgical refining technologies by Ichikawa and Cho [4,5], we think they can be simply divided into two categories depending on the form of tramp element containing phase removed from the raw material: (1) in the form of solid intermetallic compounds [6–8] and (2) in the form of liquid phase [9]. The method used in this study belongs to the later one. Those tramp elements will melt and

aggregate to the grain boundaries of solid primary aluminum at high temperatures under the melting point of aluminum. Thus a semi-solid system can be obtained and with certain solid/liquid separation treatment the tramp elements can be removed from the primary aluminum phase. Then the aluminum alloy scraps can be refined and recycled.

Flemings has first introduced the semi-solid processing (also called the partial/fractional solidification or the rheorefining process) into the purification of metal alloy scrap [10]. In the rheorefining process, alloy scraps are heated to the solid/liquid coexisting temperature range. When the volume fraction of solid is small and the solid phases are oxides, nonmetallic inclusions or other particulates with high melting point, the separation can be accomplished effectively by filtration treatment [11,12], electromagnetic force [13–17] or gravitational sedimentation [18]. For example, to separate the Fe-Al-Si or Si solid phases from aluminum melt. However, when the volume fraction of solid is large, then the liquid phase is interspersed in the grain boundaries or interdendritic space, where impurities of low melting point are invaded and accumulated. The liquid phase is so finely dispersed that it is difficult to be removed from the dendritic solid. Ichikawa has investigated the rheorefining process of Al-Sn and Al-Ni alloys to obtain high-purity aluminum assisted by the mechanical squeeze [4]. However, the plunger speed was just about  $2.8 \times 10^{-4}$  mm/s and the total squeezing time had reached to 72 ks. And it has high requirement on the components like plungers. Cho etc. have performed comprehensive investigation on purification of aluminum alloys by backward extrusion process, but we think the refining effect may deteriorate quickly when applied to large scale experiments and the loss of aluminum is high for this method [5,19,20]. In the present work, for the aim of further enhancing the segregation tendency of liquid phase from grain boundaries and improving the separation efficiency, the super-gravity field generated by centrifugation was introduced in the rheorefining process of 7075 aluminum alloys.

Song has investigated the removal of nonmetallic inclusions from liquid aluminum by super-gravity [21,22]. Those nonmetallic inclusions have high melting point and the separation temperature can be easily controlled between the melting points of inclusions and aluminum. While in this study, in order to improve the flowability of liquid intermetallic compounds and keep the aluminum matrix in solid state, the separation temperature should be kept a little lower than the melting point of aluminum. Li has used the super-gravity field to separate valuable components from metallurgical slags [23–25]. The separation temperature in his study was usually above 1300 °C, which called high requirement on apparatus and experiment operation. Moreover, oxide melts usually have high viscosity and low flowability compared to liquid metals. In view of this point, it is more suitable to use the super-gravity technology in the separation treatment of molten metal system. It has been known that in super-gravity field, the interfacial and surface tensions of liquid phase are negligible. Then the flowability of the viscous fluid phase can be improved enormously and the separation efficiency can be improved simultaneously. With the help of super-gravity field, the liquid phase of low melting point will be drained from the Al-enriched solid phase in the form of small liquid drops [26]. Thus, the liquid contaminated with impurities could be separated effectively from the semi-solid alloy through a filter. However, few literatures can be found investigating the super-gravity aided rheorefining of wrought aluminum alloys. The influence of separation temperature/time, gravity coefficient and the detailed removal mechanism of tramp elements in this system are still unknown. Thus, we carried out this investigation and try to clarify above issues.

## 2. Materials and Methods

In this study, the wrought 7075 aluminum alloy was selected as the experimental material, which has high strength and is usually used for aerospace and structural engineering. The composition of the raw material was determined by ICP-OES analysis and the result is listed in Table 1. The 7075 raw materials used in this study were rods of 17 mm in diameter and 30 mm in height divided from lump material using electric-arc cutting. The experimental apparatus and the rheorefining process are illustrated in Figure 1. The experimental apparatus are mainly composed of an electric furnace

and a centrifugal system. The two-stage graphite crucible with a porous support plate was used to complete the filtration process. The graphite felt of 5 mm in thickness 20 mm in diameter and 0.12–0.14 in volume density was used as the filter (the same as reference 25).

**Table 1.** Chemical composition of 7075 used in this study.

Element	Si	Fe	Cu	Mg	Mn	Cr	Zn	Al
Content/wt %	<0.1	0.15	1.7	2.9	0.9	0.18	6.2	Bal.

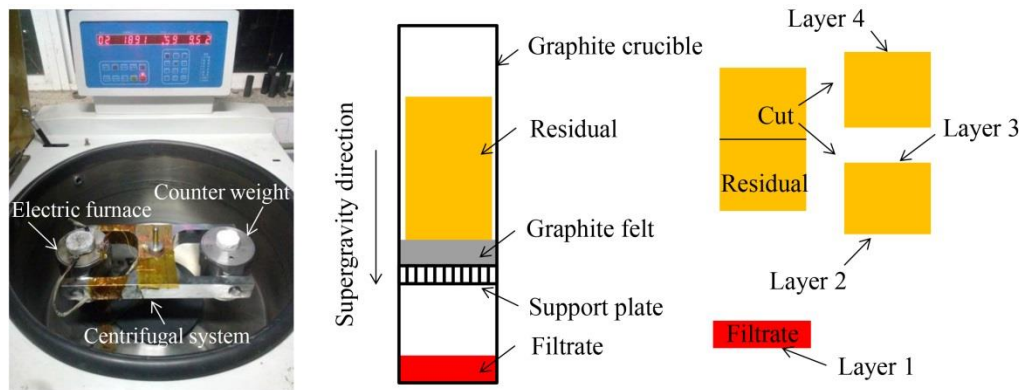


**Figure 1.** Sketch map of the super-gravity rheofining apparatus.

The experimental procedure is as follows. First of all, the electric furnace was heated to the preset temperature (the temperatures used in this study are shown in Table 2). A 7075 billet was put into the upper part of the two-stage graphite crucible and kept in the electric furnace for 20 min to achieve a solid/liquid coexisting state. Then the centrifugal system was turned on with a certain gravity coefficient. After the centrifugal treatment with a fixed time, the samples were taken out and cooled in air. The upper sample is the residual and the lower sample is the filtrate. The residual part was equally cut into two parts transversely. Finally, all the samples were grinded and polished for following Scanning Electron Microscope (SEM) and Energy Dispersive Spectrum (EDS) analysis. Four layers were chosen to be observed as illustrate in Figure 1. It was proved that the element content detected by EDS was very close to that determined by ICP-OES analysis after separation processing. Thus, every value of element was derived from the average values of three EDS results in this experiment. Totally 11 trials were carried out in this experiment. The experimental conditions are shown in Table 2. The range of the semi-solid temperature of 7075 was determined to be 475–640 °C [19,27], the separation temperatures in this study were selected as 609 °C, 617 °C and 625 °C. And the gravity coefficients were selected as 400 G, 700 G, 1000 G. The gravity coefficient was calculated as the ratio of super-gravitational acceleration to gravitational acceleration via Equation (1) [28]. Where  $G$  is the gravity coefficient,  $N$  is the rotating speed of the centrifugal (r/min),  $R$  the distance from the centrifugal axis to the center of sample,  $R = 0.25$  m,  $g = 9.8$  m/s<sup>2</sup>. The holding time is the time that the sample was kept in the electric furnace for heating. The separation time is the duration that the sample was subjected in the super-gravity filed.

$$G = \frac{\sqrt{g^2 + (\omega^2 R^2)}}{g} = \frac{\sqrt{g^2 + \left(\frac{N^2 \pi^2 R}{900}\right)}}{g} \quad (1)$$

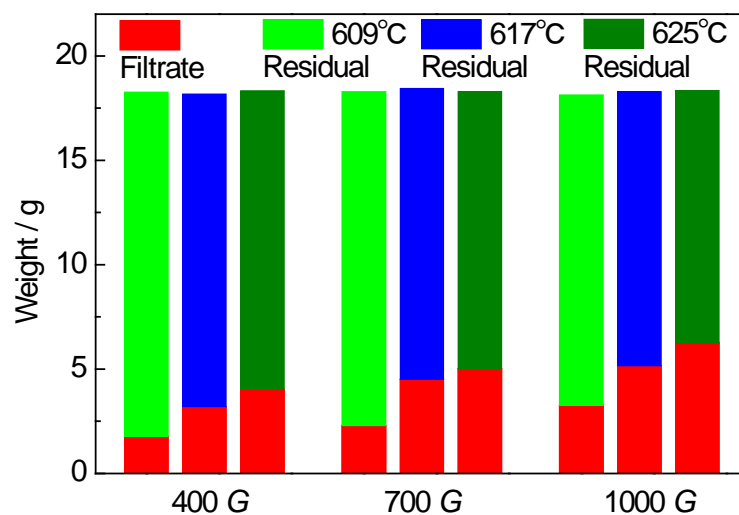
**Table 2.** Experimental conditions used in this study.

Trials	Temperature (°C)	Gravity Coefficient	Holding Time (min)	Separation Time (min)
1	609	400	20	5
2	609	700	20	5
3	609	1000	20	5
4	617	400	20	5
5	617	700	20	5
6	617	1000	20	5
7	625	400	20	5
8	625	700	20	5
9	625	1000	20	5
10	625	700	20	1
11	617	1	25	0

### 3. Results

#### 3.1. Separation Effect of Solid/Liquid Phases

The separation process was carried out according to the introduction in Section 2, after which the filtrate and residual parts were obtained. They were weighed and the result is shown in Figure 2. The total weight was basically constant before and after separation which was about 18.3 g. The weight of filtrates increased both with the enhancement of gravity coefficient and temperature. The minimum weight of filtrate was obtained in trial 1 (1.8 g, 609 °C, 400 G) and the maximum was obtained in trial 9 (6.3 g, 625 °C, 1000 G). In trial 10 the weight of filtrate was 5.2 g and the weight of residual was 12.8 g, which is close to that in trial 8 (filtrate 5.0 g, residual 13.3 g). In trial 11 there was no filtrate obtained and the weight of residual was 18.3 g.

**Figure 2.** The weights of filtrate and residual in the trials 1–9.

#### 3.2. Morphology in Different Layers

The distribution of alloying elements in the 7075 raw material is shown in Figure 3. It can be seen that those intermetallic compounds are randomly interspersed as small particles in the matrix. The tramp elements in the raw 7075 aluminum alloy are in the form of fine inclusions evenly distributed in the matrix as shown in Figure 4a. Take trial 4 for an example, it can be found from the cross section of filtrate that it is composed of light-colored impurity phase and dark Al-enriched matrix phase. The ellipsoidal columnar crystals of the Al-enriched matrix phase distribute in the dense net shape impurity phase. It can be found that some liquid phase containing tramp elements still remained

on the grain boundaries of the residual part after separation treatment. The impurity phase in grain boundaries of the Al-enriched matrix phase decreases from layer 2 to layer 4 gradually as shown in Figure 4d–f. The SEM images in Figure 4b–e showed that the thickness and the number of grain boundaries decreased, and some grain boundaries disappeared due to the compression effect caused by super-gravity. The content of tramp elements from the top of the residual downward decreases slightly, which proves that the separation effect declines from top to bottom of the residual. This phenomenon may result from the increase of inhibition effect on the flow of liquid phase by those Al-enriched matrix grains. However, the removal effects of tramp elements in different positions are all in high level and differ just a little. Thus, the super-gravity field can help to overcome the flowing inhibition effect of Al-enriched matrix grains on the liquid phase.

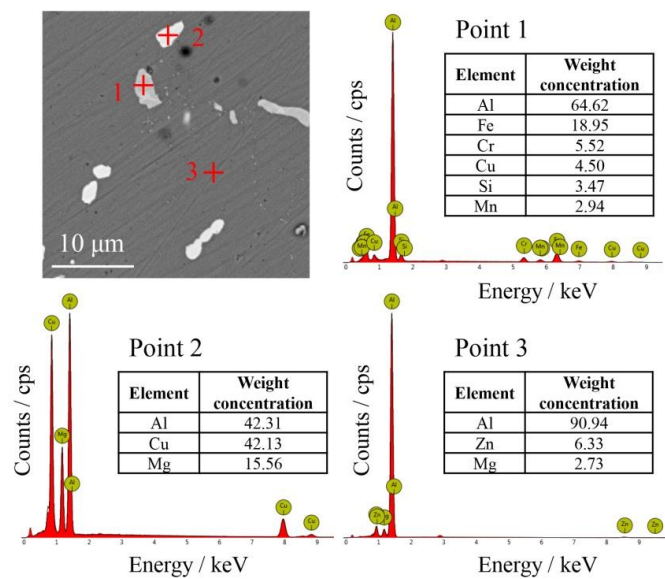


**Figure 3.** SEM and EDS analysis of the 7075 raw material.

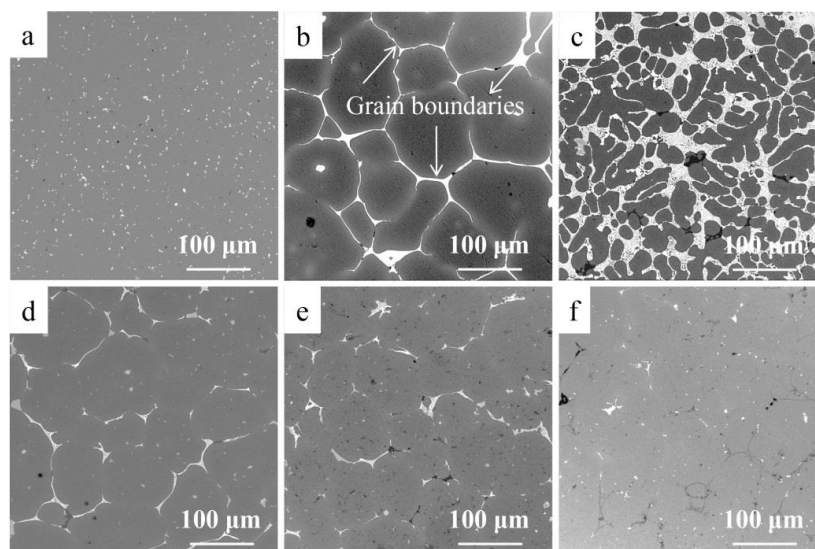


**Figure 4.** Morphology of raw material (a), after heat treatment in trail 11 (b) and different layers ((c): layer 1, (d): layer 2, (e): layer 3, (f): layer 4) in trail 4 (BSE mode).

### 3.3. The Composition and Distribution of Residual and Filtrate

The compositions of four kinds of layers as indicated in Figure 1 were analyzed with EDS. The minimum magnification was selected when proceeding the EDS analysis to reduce the error caused by the difference of phase distribution in different areas. 3 different areas in each layer were analyzed and the average values of different elements were chosen as the final composition data. The composition changes of four kinds of elements Al, Zn, Cu and Mg were mainly tracked in this study. The composition data in trial 1–9 is displayed in Figure 5. It can be seen that the contents of Al in all filtrates (layer 1) are lower than the raw material, and the contents of tramp elements Zn, Cu, Mg are all increased. Regardless the gravity coefficient the content of Al reached the lowest value (about 75 wt %) at 609 °C. With the increase of temperature the content of Al in the filtrate increased and the contents of Zn, Cu, Mg decreased. The content of Al in each layer of residual scarcely varied with temperature.

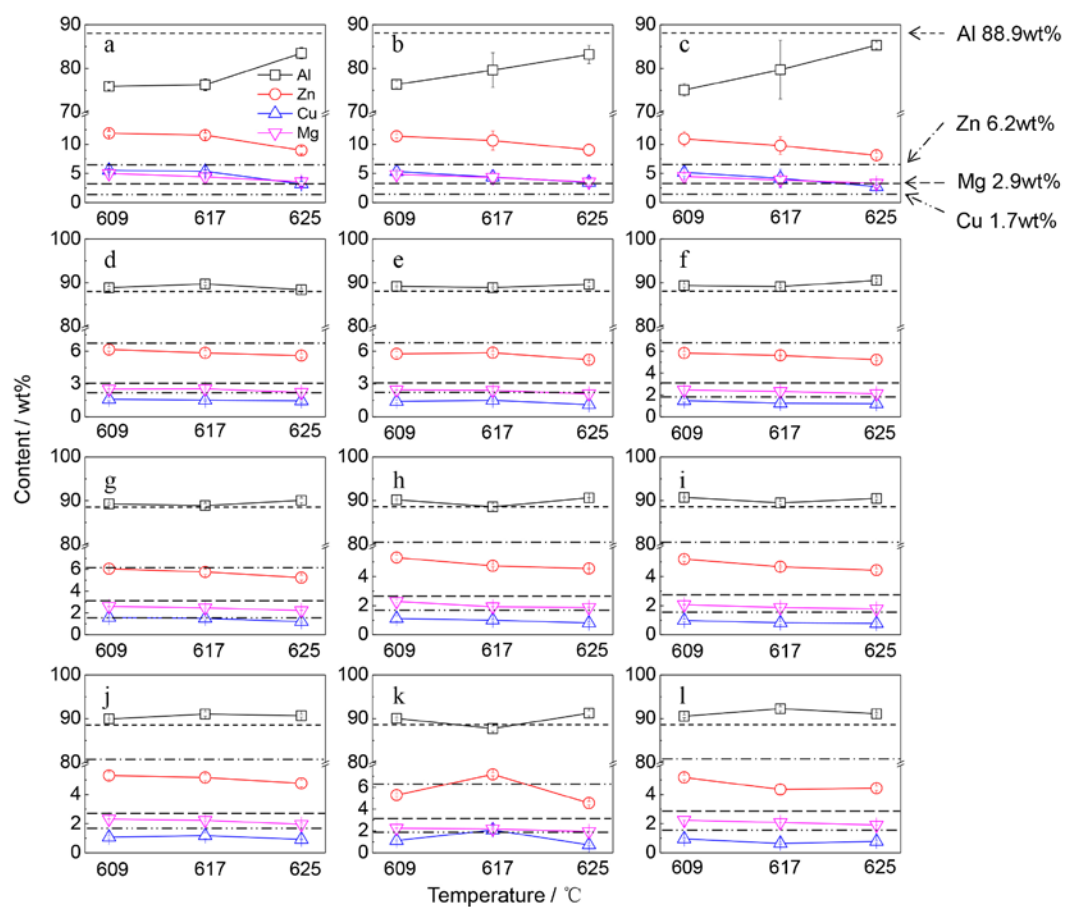


**Figure 5.** The compositions of different layers in trials 1–9: (a–c) layer 1, (d–f) layer 2, (g–i) layer 3, (j–l) layer 4, (a,d,g,j) 400 G, (b,e,h,k) 700 G, (c,f,i,l) 1000 G.

To take trial 4 as an example, the EDS mapping results of layer 1 are shown in Figure 6. In the grain boundaries of Al matrix is the net-shaped intermetallic compound zone containing Al-Zn-Cu-Mg (those four elements were mainly investigated in this study. Fe, Mn, Si, Cr may also exist in the intermetallic compound as illustrated in Figure 3). Its composition was determined with EDS spot scan as: Al 17–18 wt %, Zn 35–39 wt %, Cu 24–26 wt %, Mg 15–17 wt %. Iron is the most pervasive impurity element in aluminum alloys. The needlelike primary  $\beta$ -Fe [29] phase was found in layer 1 which composition is Al 70 wt %, Fe 20 wt %, Mn 3.2 wt %, Cr 1.0 wt %. According to the EDS mapping results, the tramp elements Fe, Mn, Cr enriched in the filtrate and it is proved that those

elements can also be removed to some extent with this method. Due to the low content of Fe, Mn, Cr and the uneven distribution of needlelike Al-Fe-Mn-Cr phases (Figure 6), which will cause large error by EDS analysis. Thus, we will track their content changes with ICP-OES method in our later study.

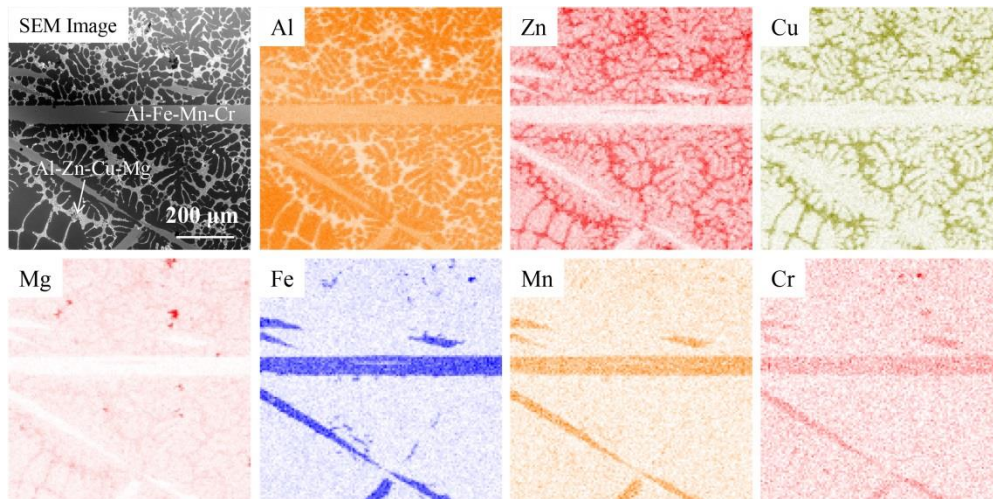


**Figure 6.** EDS mapping results of layer 1 in trial 4.

It was found that the Mg-Si-Al intermetallic phase exists in some conjunction sites of the net. As shown in Figure 7a, the dark black area as indicated by an arrow is the Mg-Si-Al phase which main composition is Mg 56 wt %, Si 36 wt %, Al 7 wt %. The fine texture of the net shape Al-Zn-Cu-Al intermetallic phase is shown in Figure 7b, which is a typical eutectic structure.

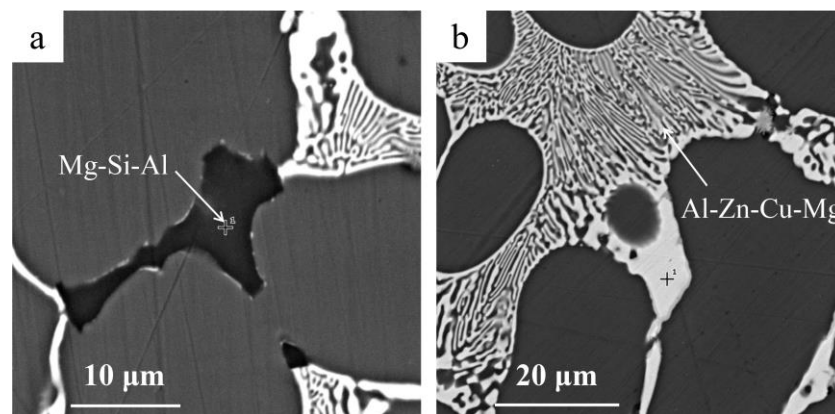


**Figure 7.** Partial enlarged views of layer 1 in trial 4 under back scattering mode. (a) Mg-Si-Al phase; (b) Al-Zn-Cu-Mg phase.

### 3.4. The Removal Ratio of Tramp Elements

The weight of Al, Zn, Cu, Mg in the filtrates can be calculated with the weight of filtrates and the contents of Al, Zn, Cu, Mg. Then the loss ratio of Al and the removal ratio of other tramp elements can be derived as:

$$R_x = \frac{m_f \cdot C_{x1}}{m_0 \cdot C_x} \quad (2)$$

where  $R_x$ : loss ratio or removal ratio;  $m_f$ : the weight of filtrate;  $C_{x1}$ : the content of Al, Zn, Cu or Mg in filtrate;  $m_0$ : the weight of original billet;  $C_x$ : the content of Al, Zn, Cu or Mg in the original billet.  $R_{Al}$  is

the loss ratio of Al, and  $R_{Zn}$ ,  $R_{Cu}$ ,  $R_{Mg}$  are the removal ratios of Zn, Cu, Mg respectively. The loss ratio of Al and the removal ratio of tramp elements all increase with the enhancement of gravity coefficient.

The driving force for the liquid phase to separate from the grain boundaries increases with the increase of gravity coefficient, then more filtrate can be obtained. Though the content of tramp elements in the filtrate decreases a little with the increase of gravity coefficient as shown in Figure 5a–c, the removal ratio of tramp elements still increases as illustrated in Figure 8b–d. The rise of separation temperature will increase the amount of liquid phase and subsequently more filtrate will be obtained. As the main component in filtrate is aluminum the rise of separation temperature will cause the increase of aluminum loss ratio.

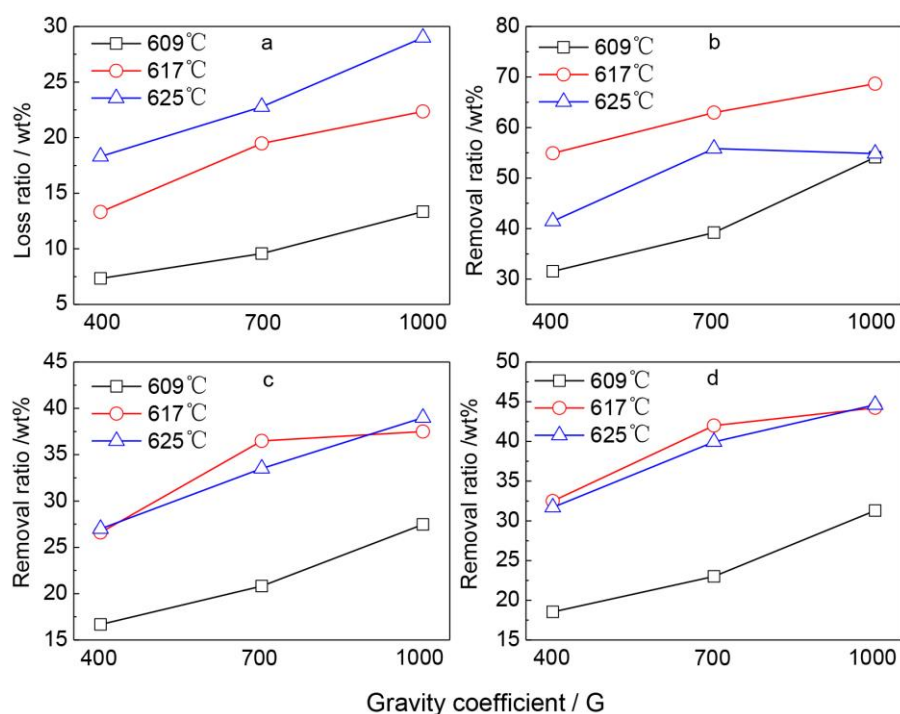


**Figure 8.** Loss ratio of Al phase (a) and removal ratio of tramp elements ((b): Cu, (c): Mg, (d): Zn).

## 4. Discussion

### 4.1. Effect of Separation Temperature

The increase of separation temperature will increase the amount of liquid phase and improve its flowability, which will lead to the increase of the filtrate amount. According to the study of Ahmad and Cho, the solid fractions corresponding to each temperature in this work are 0.8 (609 °C), 0.72 (617 °C), 0.6 (625 °C) [19,27]. The weight ratio of the residual accounting for the total weight is close to the theoretical solid fraction at the gravity coefficient of 1000 G. Thus, it is proved that the solid/liquid separation ratio with 1000 G is close to the theoretical value of solid/liquid fraction at different experimental temperatures. As shown in Figure 5, the content of aluminum decreases and the content of tramp element increases in filtrate with lower separation temperature. But the amount of liquid phase will decrease and the diffusion speed of tramp elements will drop with lowered separation temperature. Meanwhile, the flowability of liquid phase will decrease. All those above reasons will cause the less amount of filtrate obtained. Thus, the total removal ratio of tramp element decreases with lower separation temperature as shown in Figure 8. With the rise of temperature the solid grains of Al-enriched phase in the residual tended to fuse and left less voids, which can be reflected by comparison of Figures 4 and 9.

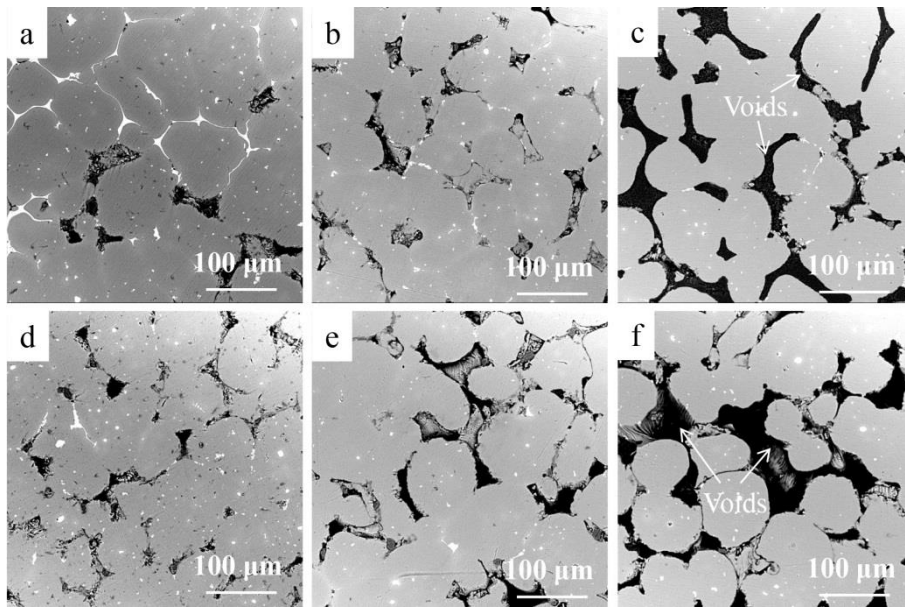


**Figure 9.** Morphology of layer 3 ((a): 400 G; (b): 700 G; (c): 1000 G) and layer 4 ((d): 400 G; (e): 700 G; (f): 1000 G) in the residual part (609 °C).

4.2. Effect of Gravity Coefficient

The separation rate of solid/liquid phases grows as the increase of gravity coefficient [22], resulting in higher weight of filtrate and dilution of tramp elements in filtrate. Thus, the contents of tramp elements Zn, Cu and Mg decrease slightly with the increase of gravity coefficient as shown in Figure 10. The net shape intermetallic phase in the filtrate becomes sparser with the increase of gravity coefficient as shown in Figure 11, which indicates that the tramp elements are diluted in the filtrate with heightened gravity coefficient. As shown in Figure 9, there were some voids observed in the intercrystalline space on layer 3 and 4 when the separation temperature was 609 °C. Those voids were left after the liquid phase flowed away. The softening trend of the Al-enriched phase was so weak that it kept its original shape and did not fill the voids. The size of the voids increases significantly with the growing of gravity coefficient. The larger size of voids corresponds to larger weight of filtrate.

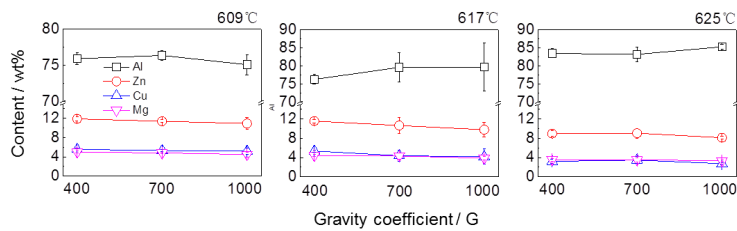


**Figure 10.** The compositions of filtrates obtained under different gravity coefficients.

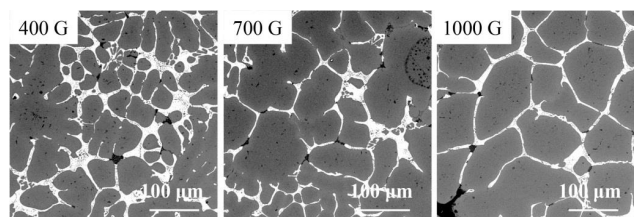


**Figure 11.** Morphology of layer 1 in the filtrate part (625 °C, backscattered electron mode (BSE)).

### 4.3. Effect of Separation Time

The experiment with the separation time of 1 min was carried out at 625 °C with the gravity coefficient of 700 G (trail 10) to investigate the influence of separation time on the separation effect. The relevant data is very close to that of trail 8, such as the weight of filtrate, the content of tramp element on layer 1–4, the removal ratio of tramp element. It is indicated that the separation rate of solid/liquid phases has reached the maximum level and the prolonging of separation time dose no good to the separation effect. The gravity coefficient is the crucial factor for separation effect compared to separation time [23,25]. For the liquid phase, its flow trend under super-gravity field equals to the viscous resistance when the separation limitation state is reached. A specific gravity coefficient corresponds to a particular separation limitation state. The separation process under super-gravity field is very fast, which 1 min is proved to be enough in this experiment.

### 4.4. Removal Mechanism of Tramp Element

7075 aluminum alloy is a kind of cold forged alloy, which features with fine grains and evenly distributed tiny intermetallic inclusions. The eutectic melts with low meting point composed of tramp elements like Zn, Cu, Mg, Fe et al. will migrate to the grain boundaries of Al-enriched phase forming net shape after heat treatment, as shown in Figure 9b. The liquid of impurity phase will flow out of the alloy matrix under super-gravity treatment, as illustrated in Figure 12, then the tramp elements will be concentrated in the bottom filtrate.

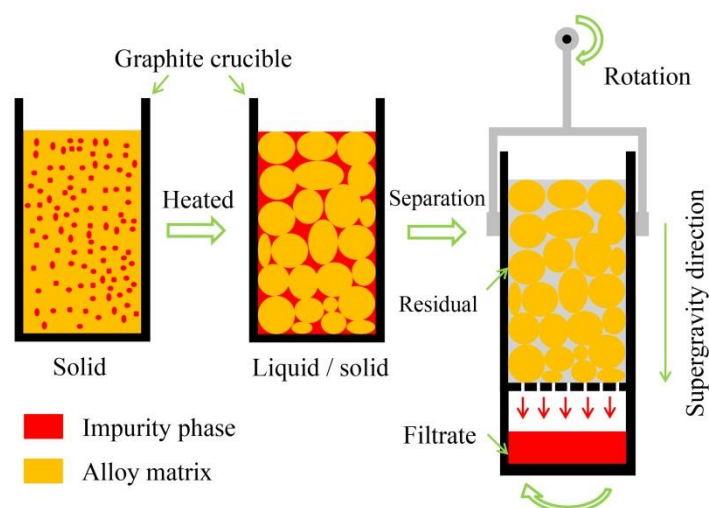


**Figure 12.** Schematic diagram of the super-gravity aided reofining process in this work.

## 5. Conclusions

11 trails were carried out in this study, influence of gravity coefficient and temperature on the separation effect and removal ratio of tramp elements are all investigated. The experimental results showed that large amount of impurities were enriched in the filtrate. Effective separation of liquid/solid phases with the aid of supergravity can be obtained within 1 min.

(1) It is proved that the tramp elements like Zn, Mg, Cu, Fe, Mn, Cr can be separated partly from the Al-enriched matrix phase using this super-gravity aided reofining method. The increase of separation temperature will lead to the increase of filtrate amount and total removal ratio of tramp elements.

(2) The separation process can be extremely accelerated in the super-gravity field, which makes great influence on the flowability of the eutectic melt containing impurities. Larger gravity coefficient will lead to higher weight of filtrate and dilution of tramp elements in filtrate.

(3) The sufficient aggregation of tramp elements in the eutectic phase of low melting point is crucial to improve the removal ratio of impurities. The separation process in the super-gravity field is so short and only 1 min of separation time is enough in this experiment.

**Author Contributions:** L.G. designed the experiments, analyzed the results and wrote this manuscript; X.W. and Q.B. helped performing most experiments; Z.G. gave some constructive suggestions on this work and helped designing the experiments.

**Funding:** This research was funded by the Fundamental Research Funds for the Central Universities FRF-TP-16-037A1 and the Key Projects of the State Key Research and Development Plan of China 2016YFB0601304.

**Conflicts of Interest:** The authors declare no conflict of interest.

## References

1. Moore, J.J. Recycling of non-ferrous metals. *Int. Met. Rev.* **1978**, *23*, 241–264. [[CrossRef](#)]
2. Gao, J.W.; Shu, D.; Wang, J.; Sun, B.D. Study on iron purification from aluminium melt by  $\text{Na}_2\text{B}_4\text{O}_7$  flux. *Mater. Sci. Technol.* **2009**, *25*, 619–624. [[CrossRef](#)]
3. Chen, C.; Wang, J.; Shu, D.; Zhang, S.; Sun, B.D. Removal of non-metallic inclusions from aluminum by electroslag refining. *Mater. Trans.* **2011**, *52*, 2266–2269. [[CrossRef](#)]
4. Ichikawa, K.; Katoh, M.; Asuke, F.; Nakazawa, Y. High efficient recovery of pure aluminum from Al-Sn and Al-Ni alloys by rheorefining process. *Mater. Trans.* **1997**, *38*, 622–629. [[CrossRef](#)]
5. Cho, T.T.; Sugiyama, S.; Yanagimoto, J. Effect of process parameters on purification of aluminium alloys by backward extrusion process under a semisolid condition. *Mater. Trans.* **2016**, *57*, 404–409. [[CrossRef](#)]
6. Kim, S.W.; Im, U.H.; Cha, H.C.; Kim, S.H.; Jang, J.E.; Kim, K.Y. Removal of primary iron rich phase from aluminum-silicon melt by centrifugal separation. *China Foundry* **2013**, *10*, 112–117. [[CrossRef](#)]
7. Shu, D.; Li, T.X.; Sun, B.D.; Zhou, Y.H.; Wang, J.; Xu, Z.M. Numerical calculation of the electromagnetic expulsive force upon nonmetallic inclusions in an aluminum melt: Part II. Cylindrical particles. *Metall. Mater. Trans. B* **2000**, *31*, 1535–1540. [[CrossRef](#)]
8. Shu, D.; Li, T.X.; Sun, B.D.; Zhou, Y.H.; Wang, J.; Xu, Z.M. Numerical calculation of the electromagnetic expulsive force upon nonmetallic inclusions in an aluminum melt: Part I. Spherical particles. *Mater. Trans. B* **2000**, *31*, 1527–1533. [[CrossRef](#)]
9. Hashimoto, E.; Ueda, Y. Zone refining of high-purity aluminum. *Mater. Trans.* **1994**, *35*, 262–265. [[CrossRef](#)]
10. Mehrabian, R.; Geiger, D.R.; Flemings, G.A. Refining by partial solidification. *Mater. Trans.* **1974**, *5*, 785–787. [[CrossRef](#)]
11. de Moraes, H.L.; de Oliveira, J.R.; Espinosa, D.C.R.; Tenório, J.A.S. Removal of iron from molten recycled aluminum through intermediate phase filtration. *Mater. Trans.* **2006**, *47*, 1731–1736. [[CrossRef](#)]
12. Kennedy, M.W.; Akhtar, S.; Bakken, J.A.; Aune, R.E. Electromagnetically modified filtration of aluminum melts-part I: Electromagnetic theory and 30 PPI ceramic foam filter experimental results. *Metall. Mater. Trans. B* **2013**, *44*, 691–705. [[CrossRef](#)]
13. Kim, J.H.; Yoon, E.P. Elimination of Fe element in A380 aluminum alloy scrap by electromagnetic force. *J. Mater. Sci. Lett.* **2000**, *19*, 253–255. [[CrossRef](#)]
14. Xu, Z.M.; Li, T.X.; Zhou, Y.H. Elimination of Fe in Al-Si cast alloy scrap by electromagnetic filtration. *J. Mater. Sci.* **2003**, *38*, 4557–4565. [[CrossRef](#)]
15. Lee, G.C.; Kim, M.G.; Park, J.P.; Lim, J.H.; Jung, J.H.; Baek, E.R. Iron Removal in aluminum melts containing scrap by electromagnetic stirring. *Mater. Sci. Forum* **2010**, *638–642*, 267–272. [[CrossRef](#)]
16. He, Y.J.; Li, Q.L.; Liu, W. Separating effect of a novel combined magnetic field on inclusions in molten aluminum alloy. *Metall. Mater. Trans. B* **2012**, *43*, 1149–1155. [[CrossRef](#)]
17. He, Y.J.; Li, Q.L.; Liu, W. Effect of combined magnetic field on the eliminating inclusions from liquid aluminum alloy. *Mater. Lett.* **2011**, *65*, 1226–1228. [[CrossRef](#)]
18. Zhao, L.X.; Guo, Z.C.; Wang, Z.; Wang, M.Y. Removal of low-content impurities from Al by super-gravity. *Metall. Mater. Trans. B* **2010**, *41*, 505–508. [[CrossRef](#)]
19. Cho, T.T.; Sugiyama, S.; Yanagimoto, J. Effect of process parameters of backward extrusion by servo press on purification of A7075 alloy under the semisolid condition. *Mater. Trans.* **2016**, *57*, 1351–1356. [[CrossRef](#)]

20. Sugiyama, S.; Meng, Y.; Yanagimoto, J. Refining and recycling of metal scraps by semisolid processing. *Solid State Phenom.* **2012**, *192–193*, 494–499. [[CrossRef](#)]
21. Song, G.Y.; Song, B.; Yang, Z.B.; Yang, Y.H.; Zhang, J. Removal of inclusions from molten aluminum by supergravity filtration. *Metall. Mater. Trans. B* **2016**, *47*, 3435–3445. [[CrossRef](#)]
22. Song, G.Y.; Song, B.; Yang, Z.B.; Yang, Y.H.; Xin, W.B. Separating behavior of nonmetallic inclusions in molten aluminum under super-gravity field. *Metall. Mater. Trans. B* **2015**, *46*, 2190–2197. [[CrossRef](#)]
23. Li, C.; Gao, J.T.; Guo, Z.C. Isothermal enrichment of P-concentrating phase from CaO–SiO<sub>2</sub>–FeO–MgO–P<sub>2</sub>O<sub>5</sub> melt with super gravity. *ISIJ Int.* **2016**, *56*, 759–764. [[CrossRef](#)]
24. Li, C.; Gao, J.T.; Wang, F.Q.; Guo, Z.C. Enriching Fe-bearing and P-bearing phases from steelmaking slag melt by super gravity. *Ironmak. Steelmak.* **2016**, *45*, 1–6. [[CrossRef](#)]
25. Li, J.C.; Guo, Z.C.; Gao, J.T. Laboratory assessment of isothermal separation of V containing spinel phase from vanadium slag by centrifugal casting. *Ironmak. Steelmak.* **2014**, *41*, 710–714. [[CrossRef](#)]
26. Yang, H.J.; Chu, G.W.; Zhang, J.W.; Shen, Z.G.; Chen, J.F. Micromixing efficiency in a rotating packed bed: experiments and simulation. *Ind. Eng. Chem. Res.* **2005**, *44*, 7730–7737. [[CrossRef](#)]
27. Ahmad, A.H.; Naher, S.; Brabazon, D. Thermal profiles and fraction solid of aluminium 7075 at different cooling rate conditions. *Key Eng. Mater.* **2013**, *554–557*, 582–595. [[CrossRef](#)]
28. Li, J.C.; Guo, Z.C.; Gao, J.T. Isothermal enriching perovskite phase from CaO–TiO<sub>2</sub>–SiO<sub>2</sub>–Al<sub>2</sub>O<sub>3</sub>–MgO melt by super gravity. *ISIJ Int.* **2014**, *54*, 743–749. [[CrossRef](#)]
29. Cao, X.; Campbell, J. The solidification characteristics of Fe-rich intermetallics in Al-11.5Si-0.4Mg cast alloys. *Metall. Mater. Trans. A* **2004**, *35*, 1425–1435. [[CrossRef](#)]



© 2018 by the authors. Licensee MDPI, Basel, Switzerland. This article is an open access article distributed under the terms and conditions of the Creative Commons Attribution (CC BY) license (<http://creativecommons.org/licenses/by/4.0/>).